ISSN 0023-1584, Kinetics and Catalysis, 2007, Vol. 48, No. 1, pp. 143–152. © MAIK "Nauka/Interperiodica" (Russia), 2007.
Original Russian Text © G.A. Turko, A.S. Ivanova, L.M. Plyasova, G.S. Litvak, V.A. Rogov, E.M. Slavinskaya, I.A. Polukhina, A.S. Noskov, 2007, published in Kinetika i Kataliz, 2007, Vol. 48, No. 1, pp. 150–160.

Dependence of the Properties of Ce–Zr–Y–La–M–O Systems on Synthetic Conditions and on the Nature of the Transition Metal M (Mn, Fe, Co)

G. A. Turko, A. S. Ivanova, L. M. Plyasova, G. S. Litvak, V. A. Rogov, E. M. Slavinskaya, I. A. Polukhina, and A. S. Noskov

Boreskov Institute of Catalysis, Siberian Branch, Russian Academy of Sciences, Novosibirsk, 630090 Russia
e-mail: iva@catalysis.nsk.su

Received May 23, 2005

Abstract—The effects of synthetic conditions, component ratios, and the nature of the transition metal on the physicochemical and catalytic properties of Ce–Zr–Y–La–M–O (M = Mn, Fe, Co) systems are studied. The Ce–Zr–Y–La–M–O samples precipitated at ~23°C and calcined at 600°C are single-phase and are solid solutions with a fluorite structure, which persists upon calcination at 1150°C. The Ce–Zr–Y–La–Fe(Co)–O samples precipitated at 70°C and calcined at 1150°C consist of two solid solutions, one cubic, and the other tetragonal. The specific surface area (S_{sp}) of the samples precipitated at ~23°C and calcined at 600°C increases in the order Ce–Zr–Y–La–O < Ce–Zr–Y–La–Mn–O < Ce–Zr–Y–La–Co–O ≈ Ce–Zr–Y–La–Fe–O. The specific surface area of the samples precipitated at 70°C is independent of M and is ~110 m^2/g. Calcination at 1150°C reduces S_{sp} approximately by two orders of magnitude. The TPR of the unpromoted systems in H_2 proceeds in two steps at 600–650 and 750–840°C. The introduction of M decreases the reduction temperatures and gives rise to a lower temperature peak between 150 and 300°C. The most effective promoter is cobalt. The fluorite-type catalysts containing no noble metal are active in NO reduction ($X_{NO} \approx 100\%$) at T_{react} = 400–450°C. The cobalt-containing catalysts are the most active in the oxidation of CO ($X_{max} = 28\%$) and hydrocarbons ($X_{max} = 4.3\%$).

DOI: 10.1134/S0023158407010193

In recent years, much attention has been focused on so-called three-way catalysts (TWCs, Pt(Pd)/$Ce_{1-x}Zr_xO_{2-x}$/support), which serve to simultaneously convert the hydrocarbons, CO, and NO_x in automotive exhaust. The conditions under which these catalysts operate are specific in that the composition of the exhaust gas is unsteady because of the variation of the fuel/air ratio. The catalysts are known to be most efficient when the ratio between the oxidizing and reductive components in the gas mixture is stoichiometric [1]. Deviations from stoichiometry reduce the activity of the catalyst [2, 3]. Therefore, new approaches to the formulation and synthesis of automotive catalysts are necessary. A possible approach is to promote the cerium–zirconium oxide system with rare-earth and transition metal cations [4–6] in order to enhance both thermal stability and activity.

Among the rare-earth metals, yttrium and lanthanum are the most appropriate for stabilizing the fluorite structure of the Ce–Zr–O compositions [4, 7]. Introducing their cations into $Ce_{1-x}Zr_xO_{2-x}$ stabilizes the cubic structure at a low cerium dioxide content (30 mol %). The resulting solid solutions have a comparative high oxygen storage capacity, as is indicated by hydrogen temperature-programmed reduction (TPR) data [4].

The reduction of the cerium–zirconium oxide systems is also affected by transition metal cations. The introduction of a transition metal into CeO_2 or a Ce–Zr–Y–O composition decreases the reduction temperature [5, 8]. Introducing 0.6 wt % NiO into Ce–Zr–O shifts the reduction peaks to slightly lower temperatures of 270 and 380°C, and raising the NiO content to 12.4 wt % decreases the corresponding reduction temperatures to 180 and 320°C [9]. It is, therefore, likely that transition metals will increase the number of vacancies, since their valence is lower than the valence of the cerium or zirconium cation. Furthermore, the redox properties of the system will be determined by both the Ce^{4+}/Ce^{3+} couple and the M^{3+}/M^{2+} couple.

The purpose of this study was to obtain a fluorite-type single-phase composition based on the Ce–Zr–Y–La–O system and promoted by transition metal cations (M = Mn, Fe, Co) and to study its catalytic and physicochemical properties.

EXPERIMENTAL

Initial systems were precipitated from solutions of appropriate amounts of metal nitrates with aqueous ammonia at room and elevated temperatures (~23 and 70°C). The exceptions were the cobalt-containing sys-

Table 1. Effect of the catalyst composition on the constitutional water content

Sample composition	T_{precip}, °C	Designation	H_2O, mol/(mol solid)		Δ, mol/(mol solid)
			110–600°C	110–900°C	
$Ce_{0.18}Zr_{0.69}Y_{0.09}La_{0.04}O_{1.94}$	~23	**$Ce_{0.18}Zr_{0.69}$(23)**	**0.76**	**0.92**	**0.16**
$Ce_{0.21}Zr_{0.64}Y_{0.09}La_{0.04}Mn_{0.03}O_{1.92}$		$Ce_{0.21}Zr_{0.64}$Mn(23)	0.77	0.86	0.09
$Ce_{0.20}Zr_{0.64}Y_{0.09}La_{0.04}Fe_{0.03}O_{1.92}$		$Ce_{0.20}Zr_{0.64}$Fe(23)	0.80	0.83	0.03
$Ce_{0.22}Zr_{0.61}Y_{0.10}La_{0.04}Co_{0.03}O_{1.91}$		$Ce_{0.22}Zr_{0.61}$Co(23)	0.80	0.83	0.03
$Ce_{0.35}Zr_{0.51}Y_{0.10}La_{0.04}O_{1.93}$		**$Ce_{0.35}Zr_{0.51}$(23)**	**0.72**	**0.90**	**0.18**
$Ce_{0.34}Zr_{0.49}Y_{0.09}La_{0.04}Mn_{0.04}O_{1.92}$		$Ce_{0.34}Zr_{0.49}$Mn(23)	0.85	0.95	0.10
$Ce_{0.33}Zr_{0.51}Y_{0.09}La_{0.04}Fe_{0.03}O_{1.92}$		$Ce_{0.33}Zr_{0.51}$Fe(23)	0.83	0.91	0.08
$Ce_{0.32}Zr_{0.52}Y_{0.09}La_{0.04}Co_{0.03}O_{1.92}$		$Ce_{0.32}Zr_{0.52}$Co(23)	0.88	0.90	0.02
$Ce_{0.30}Zr_{0.55}Y_{0.07}La_{0.05}Mn_{0.03}O_{1.93}$	70	$Ce_{0.30}Zr_{0.55}$Mn(70)	0.95	1.15	0.20
$Ce_{0.29}Zr_{0.57}Y_{0.07}La_{0.04}Fe_{0.03}O_{1.93}$		$Ce_{0.29}Zr_{0.57}$Fe(70)	0.95	1.11	0.16
$Ce_{0.30}Zr_{0.57}Y_{0.07}La_{0.04}Co_{0.02}O_{1.94}$		$Ce_{0.30}Zr_{0.57}$Co(70)	0.96	1.07	0.11

tems, which were precipitated with aqueous KOH (2 N) for the reason that cobalt ammines are soluble. The resulting slurries were filtered, and the cakes were washed with distilled water until the filtrate was free of the nitrate ion. The resulting solids were dried in air and then in an oven at 110°C for 12–14 h. Next, the solids were heat-treated in flowing dry air at 600°C for 2 h and then in a muffle furnace at 1150°C for 12 h.

The systems were analyzed for main components by atomic absorption spectroscopy [10]. The constitutional water content was derived from calcination loss data. The calcination loss was determined as the ratio of the weight of a sample dried at 110°C for 1 day minus the weight of the same sample calcined at 600 or 900°C for 4 h to the initial sample weight.

Thermal analysis was carried out in air on a Q1500D or DTG-60H (Shimadzu) thermoanalytical system. The sample weight was 500 mg (Q1500D) or 40 mg (DTG-60H). The samples were heated from 18–21 to 1200°C at a rate of 10 K/min. The temperature was measured with an accuracy of ±5 K; weight loss, with an accuracy of ±1%.

X-ray diffraction phase analysis was carried out with a URD-63 diffractometer using CuK_α radiation filtered with a graphite monochromator in the reflected beam. Diffraction patterns were obtained by scanning the $2\theta = 10°–60°$ range with $\tau = 0.05$ (2θ) increments at a count time of 5 s per point. Unit 6 cell parameters were calculated by least squares using the Polikristall program package. The particle size of phases was determined by the Selyakov–Scherrer formula primarily along the (220) direction. Diffraction patterns were processed using the PCW.2.4 and Polikristall programs [11, 12].

The specific surface area was determined by the thermal Argon desorption method [13] with an accuracy of ±10%.

Hydrogen TPR was varied out in a flow reactor. The sample was heated from room temperature to 900°C at a rate of 10 K/min. The hydrogen concentration in argon was 10 vol %, and the flow rate was 40 ml/min. The resulting H_2O was frozen out at –80°C. The hydrogen was measured using a thermal-conductivity detector. The catalyst particle size was 0.25–0.50 mm, and the sample weight was 0.2 g. Prior to reduction, the samples were conditioned in oxygen at 500°C for 0.5 h.

The catalytic properties of oxide systems in CO and hydrocarbon (C_3H_6 and C_3H_8) oxidation and in NO reduction were studied in a flow reactor in terms of the conversion of the substrate into CO_2 and N_2. The reaction mixture, which consisted of 0.16–1.80 vol % O_2, 1.00 vol % CO, 0.015 vol % C_3H_6, 0.03 vol % C_3H_8, 0.35 vol % H_2, 0.15 vol % NO, 10 vol % H_2O, and He as the balance gas, was passed through a catalyst bed (0.63 cm^3; particle size, 0.25–0.50 mm) at a VHSV of 48000 h^{-1}. The reaction temperature was 400 or 450°C. The initial reaction mixture and the products were analyzed on a Tsvet-500 chromatograph (Russia); NO and NO_2 were determined using an ECOM-Omega chromatograph with NO and NO_2 detectors. We used the Katana program to control all reactor units and to collect and process reactor operation and chromatographic data. Catalysts were tested at different values of the redox potential R defined as

$$R = \frac{9[C_3H_6] + 10[C_3H_8] + [CO] + [H_2]}{2[O_2] + [NO]}.$$

RESULTS AND DISCUSSION

Chemical and Phase Composition

Table 1 lists chemical composition data for samples with different component ratios along with their short designations. The constitutional water content of these

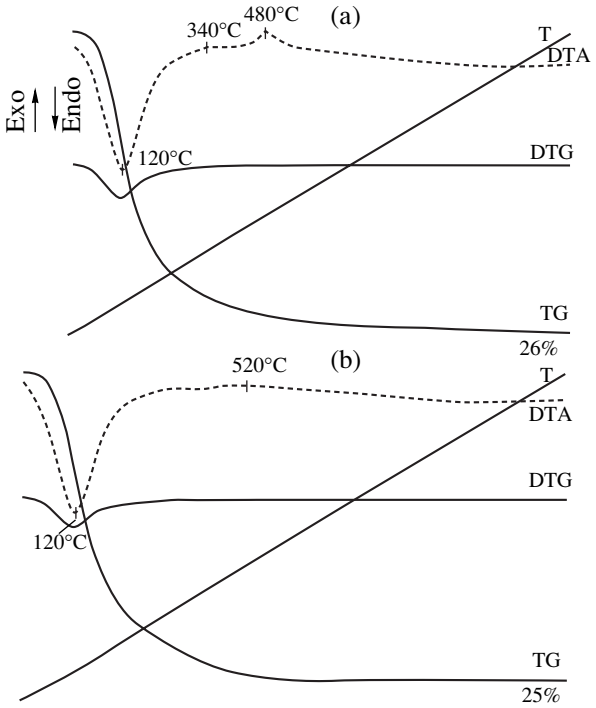

Fig. 1. Thermoanalytical data for (a) $Ce_{0.35}Zr_{0.51}$ and (b) $Ce_{0.34}Zr_{0.49}Mn$.

samples, determined from weight loss data in two temperature ranges, depends on the composition and synthetic conditions. It increases as the cerium dioxide content is increased and as the precipitation temperature is raised (Table 1). The constitutional water contents determined at 600 and 900°C differ. The difference Δ depends on the nature of the transition metal (Table 1), decreasing in the order Mn ⟶ Fe ⟶ Co for series of samples with similar compositions ($Ce_{0.20–0.22}Zr_{0.61–0.64}M$ or $Ce_{0.32–0.34}Zr_{0.51–0.55}M$). Furthermore, introducing a transition metal into the Ce–Zr–Y–La–O system favors the dehydroxylation of the surface, since most of the constitutional water is eliminated at lower temperatures (110–600°C) in the presence of a transition metal.

According to thermoanalytical data, the thermal genesis of $Ce_{0.35}Zr_{0.51}(23)$ and $Ce_{0.34}Zr_{0.49}Mn(23)$ gives rise to a low-temperature endotherm at 120°C, which is due to the elimination of physically adsorbed water, and to exotherms at 340 and 480°C for $Ce_{0.35}Zr_{0.51}(23)$ (Fig. 1a) and at 520°C for $Ce_{0.34}Zr_{0.49}Mn(23)$ (Fig. 1b). The weight losses of these samples differ only slightly, being 26 and 25% for $Ce_{0.35}Zr_{0.51}(23)$ and $Ce_{0.34}Zr_{0.49}Mn(23)$, respectively. Thus, the phase transitions in the materials examined are complete at ~500°C (Fig. 1).

Figure 2 shows the X-ray diffraction patterns from samples containing different transition metals, all obtained by precipitation at ~23°C followed by heat treatment at 600°C. The diffraction patterns from the

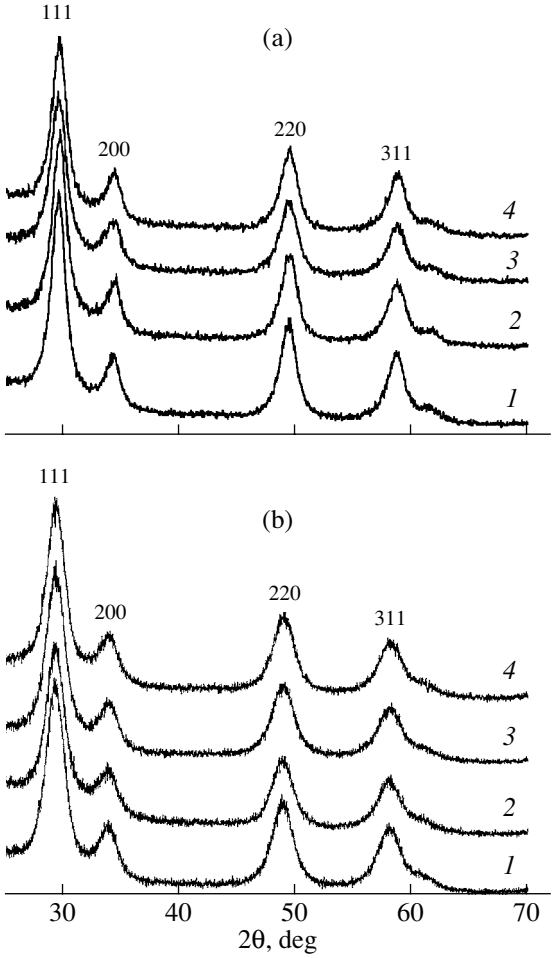

Fig. 2. X-ray diffraction patterns from samples calcined at 600°C: (a) (*1*) $Ce_{0.18}Zr_{0.69}$, (*2*) $Ce_{0.21}Zr_{0.64}Mn$, (*3*) $Ce_{0.20}Zr_{0.64}Fe$, and (*4*) $Ce_{0.22}Zr_{0.61}Co$; (b) (*1*) $Ce_{0.35}Zr_{0.51}$, (*2*) $Ce_{0.34}Zr_{0.49}Mn$, (*3*) $Ce_{0.33}Zr_{0.51}Fe$, and (*4*) $Ce_{0.32}Zr_{0.52}Co$.

Ce–Zr–Y–La–O materials show sets of reflections characteristic of a cubic phase with a fluorite structure. The unit cell parameter is 5.217 and 5.268 Å (Table 2) for $Ce_{0.18}Zr_{0.69}(23)$ (Fig. 2a) and $Ce_{0.35}Zr_{0.51}(23)$ (Fig. 2b), respectively; that is, the unit cell parameter increases with increasing cerium dioxide content (because $a_{ZrO_2} = 5.09$ Å and $a_{CeO_2} = 5.41$ Å). Introducing a transition metal (Mn, Fe, Co) into the Ce–Zr–Y–La–O system does not cause the formation of a new phase; the diffraction pattern indicates the presence only of a cubic phase (Fig. 2). However, the unit cell parameter of this phase is smaller than the initial unit cell parameter. This can be explained in terms of transition metal cations being incorporated into the lattice to form a solid solution based on the Zr–Ce–Y–La–M–O system. Raising the calcination temperature to 1150°C does not lead to any structural changes in the $Ce_{0.18}Zr_{0.69}$ solid solution either, resulting only in a slight decrease in its unit cell parameter (Table 2).

Table 2. Phase composition of samples prepared under different conditions

Sample	T_{precip}, °C	T_{calcin}, °C	Phase	Unit cell parameters, Å		D_{220}, Å
$Ce_{0.18}Zr_{0.69}$	~23	600	Cubic solid solution with a fluorite structure	5.217	–	53
		1150		–	5.213	780
$Ce_{0.21}Zr_{0.64}Mn$		600		5.211	–	52
$Ce_{0.20}Zr_{0.64}Fe$				5.214	–	50
$Ce_{0.22}Zr_{0.61}Co$				5.210	–	51
$Ce_{0.35}Zr_{0.51}$				5.268	–	43
$Ce_{0.34}Zr_{0.49}Mn$				5.273	–	44
$Ce_{0.33}Zr_{0.51}Fe$				5.265	–	40
$Ce_{0.32}Zr_{0.52}Co$				5.262	–	43
$Ce_{0.30}Zr_{0.55}Mn$	70	600	Cubic solid solution with	5.312	–	40
		1150	a fluorite-type structure	–	5.219	760
$Ce_{0.29}Zr_{0.57}Fe$			89% cubic, 11% tetragonal	–	a_c = 5.236 a_t = 3.637 c_t = 5.238	680 540
$Ce_{0.30}Zr_{0.57}Co$			96.5% cubic, 3.5% tetragonal	–	a_c = 5.228 a_t =2.628 c_t = 5.227	800 320

More profound structural changes are observed in the samples precipitated at 70°C (Figs. 3, 4, Table 2). $Ce_{0.30}Zr_{0.55}Mn$ calcined at 600 and 1150°C is again a fluorite-type solid solution (Fig. 3), but its unit cell parameter is substantially larger than the unit cell parameter of a similar sample precipitated at room temperature (Table 2). The introduction of iron or cobalt causes changes in the phase composition of the Ce–Zr–Y–La–O system (Fig. 4, curves *2*, *3*), specifically, the formation of a tetragonal phase with unit cell parameters similar to those of the equilibrium $Zr_{0.8}Ce_{0.2}O_2$ solid solution. The proportion of the tetragonal phase is higher in the presence of iron. No iron or cobalt oxide phase was detected (Fig. 4, Table 2).

The determination of the phase composition of the multicomponent systems obtained under different conditions demonstrated that precipitation at ~23°C followed by heat treatment at 600°C yields single-phase materials with a fluorite structure. Raising the heat-treatment temperature to 1150°C causes no structural changes. Precipitation at 70°C followed by heat treat-

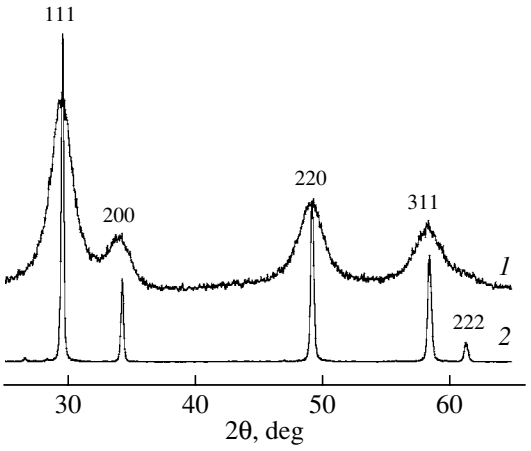

Fig. 3. X-ray diffraction pattern from $Ce_{0.30}Zr_{0.55}Mn$ precipitated at 70°C and calcined at (*1*) 600 and (*2*) 1150°C.

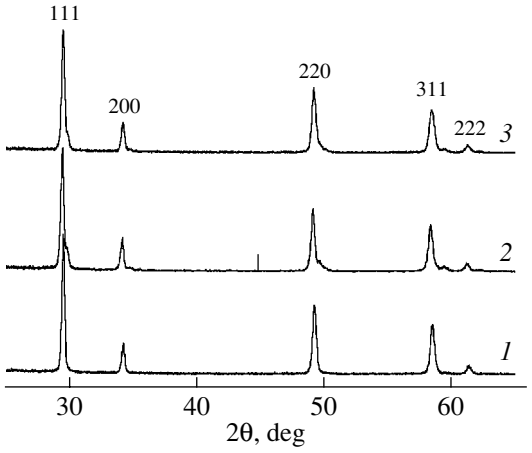

Fig. 4. X-ray diffraction pattern from samples precipitated at 70°C and calcined at 1150°C: (*1*) $Ce_{0.30}Zr_{0.55}Mn$, (*2*) $Ce_{0.29}Zr_{0.57}Fe$, and (*3*) $Ce_{0.30}Zr_{0.57}Co$.

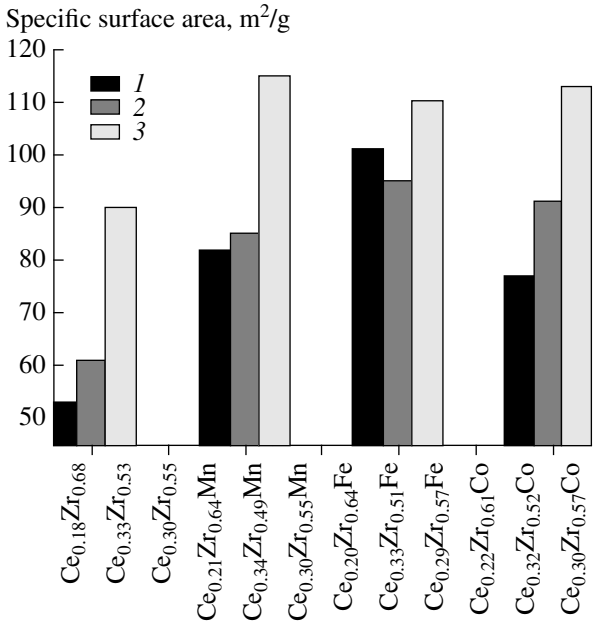

Fig. 5. Composition dependence of specific surface area for samples precipitated at (*1*, *2*) 23 and (*3*) 70°C and calcined at 600°C.

ment at 1150°C yields two-phase materials consisting of solid solutions with a cubic and a tetragonal structure (the only exception is the manganese-containing system).

The particle size (D_{220}) in the solid solution forming upon calcination at 600°C ranges between 40 and 50 Å. As the calcination temperature is raised, D_{220} increases to 700–800 Å (Table 2).

Specific Surface Area

According to adsorption data, the specific surface area S_{sp} of the systems examined depends on the synthetic and calcination temperatures. For the precipitation temperature of ~23°C and the calcination temperature of 600°C, S_{sp} increases in the order Ce–Zr–Y–La–O < Ce–Zr–Y–La–Mn–O ≈ Ce–Zr–Y–La–Fe–O < Ce–Zr–Y–La–Co–O (Fig. 5) and is almost independent of component ratios. Raising the precipitation temperature to 70°C increases S_{sp} to ~110 m²/g. These data indicate that introducing a transition metal increases S_{sp} in all cases. Calcination at 1150°C dramatically reduces S_{sp} to 0.6–0.8 m²/g for the samples precipitated at ~23°C and to 0.05–0.08 m²/g for the samples precipitated at 70°C. This difference is explained by the fact that smaller particles are more readily sinterable.

Temperature-Programmed Reduction

The hydrogen TPR data obtained in this study are of special interest. The TPR spectra have a complicated shape (Figs. 6, 7): reduction proceeds in two or three steps, depending on the sample composition, the nature of the transition metal, and the precipitation and calcination temperatures.

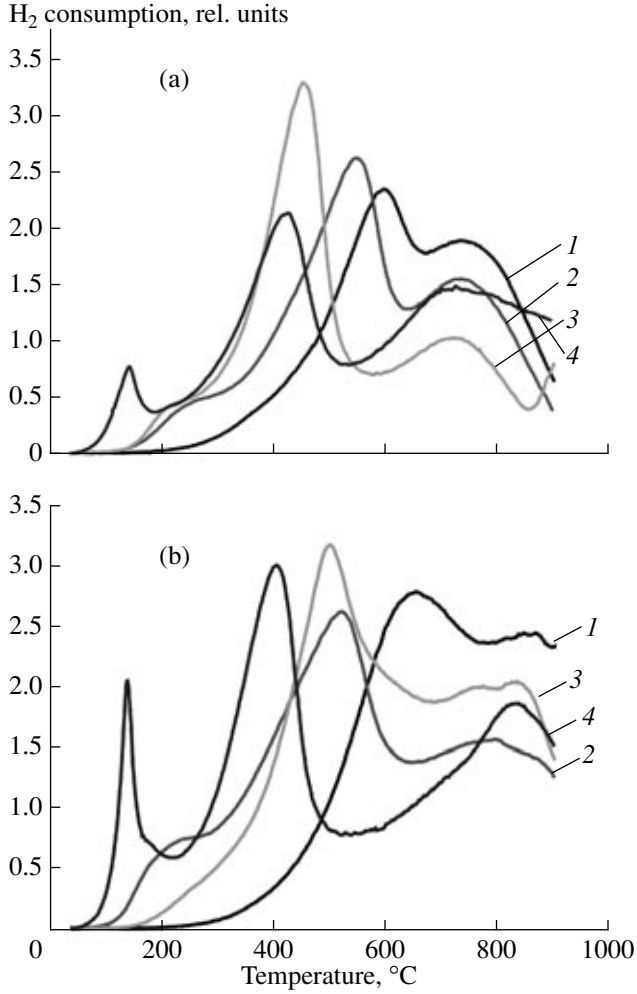

Fig. 6. TPR profiles for samples precipitated at 23°C and calcined at 600°C: (a) (*1*) $Ce_{0.18}Zr_{0.69}$, (*2*) $Ce_{0.21}Zr_{0.64}Mn$, (*3*) $Ce_{0.20}Zr_{0.64}Fe$, and $Ce_{0.22}Zr_{0.61}Co$ (*4*); (b) (*1*) $Ce_{0.35}Zr_{0.51}$, (*2*) $Ce_{0.34}Zr_{0.49}Mn$, (*3*) $Ce_{0.33}Zr_{0.51}Fe$, and (*4*) $Ce_{0.32}Zr_{0.52}Co$.

Figure 6a shows TPR profiles for samples precipitated at ~23°C and calcined at 600°C. The samples containing no transition metal are reduced in two steps, as is indicated by their reduction curves having two peaks (Figs. 6a, 6b, curves *1*) at 600 and 750°C for $Ce_{0.18}Zr_{0.69}$ and 660 and 840°C for $Ce_{0.35}Zr_{0.51}$. The peak at 600 or 660°C is due to the reduction of surface Ce^{4+} ions, and the peak at 750 or 840°C is due to Ce^{4+} reduction in the sample bulk [4, 6, 14, 15]. The introduction of transition metal cations into the cerium–zirconium oxide system brings about a low-temperature peak (Fig. 6, Table 3), whose position is determined by the transition metal.

The TPR spectrum of $Ce_{0.21}Zr_{0.64}Mn$ calcined at 600°C (Fig. 6a, curve *2*) shows three peaks at 270, 550,

Table 3. Effects of composition and synthesis temperature on the reduction behavior of the Ce–Zr–Y–La–O catalysts

Sample	T_{precip}, °C	T_{calcin}, °C	Reduction temperature, °C			H_2 consumption, mmol H_2/g		Extent of reduction*
						observed	calculated	(α)
$Ce_{0.18}Zr_{0.69}$	23	600		600	750	1.05	0.69	(1.52)
$Ce_{0.21}Zr_{0.64}Mn$			270	550	740	1.14	0.91	(1.25)
$Ce_{0.20}Zr_{0.64}Fe$			205	450	730	1.11	1.13	0.98
$Ce_{0.22}Zr_{0.61}$ëÓ			140	430	730	1.16	1.19	0.97
$Ce_{0.35}Zr_{0.51}$			–	656	841	1.31	1.24	(1.06)
$Ce_{0.34}Zr_{0.49}Mn$			215	590	800	1.37	1.34	(1.02)
$Ce_{0.33}Zr_{0.51}Fe$			500	780	840	1.55	1.57	0.99
$Ce_{0.32}Zr_{0.52}$ëÓ			140	405	840	1.39	1.49	0.93
$Ce_{0.30}Zr_{0.55}Mn$	70	600	178	505	765	1.04	1.22	0.85
$Ce_{0.30}Zr_{0.55}Mn$		1150	–	765	840	0.85	1.22	0.70
$Ce_{0.29}Zr_{0.57}Fe$			–	710	–	0.80	1.46	0.55
$Ce_{0.30}Zr_{0.57}Co$			376	761	–	0.91	1.35	0.67

* In the calculation of α, we took into account the amounts of H_2 consumed in the reduction of CeO_2 to Ce_2O_3, Mn^{4+} to Mn^{2+}, Fe^{3+} to Fe^0, and Co^{3+} to Co^0.

and 740°C. As demonstrated in earlier studies [16, 17], the reduction of MnO_2 to Mn_2O_3 proceeds as follows:

$$\begin{matrix} MnO_2 \\ Mn_2O_3 \end{matrix} \searrow\!\nearrow Mn_3O_4 \longrightarrow MnO.$$

The Mn_3O_4 phase was reported to form at 320°C; the MnO phase, at 400°C [16]. Obviously, the MnO_2 and Mn_2O_3 reduction temperatures may be different because the reducibility of the oxides depends on their modification (α, β, or γ), on the particle size, and on the nature of the salt from which the oxides were synthesized. The reduction of β-MnO_2 gives rise to peaks at 350 and 515°C, and α-MnO_2 is reduced at 320 and 400°C [18]. Evidently, all of the reduction temperatures are above 270°C. Therefore, in view of the reported data, it can be inferred that manganese cations form a surface compound that is reduced at a lower temperature than the oxides. Note that the manganese cations decrease the second peak temperature by 50°C and do not significantly shift the third peak relative to the same peak for the unpromoted sample (Table 3). In the reduction of $Ce_{0.34}Zr_{0.49}Mn$, the extra peak is observed at 215°C (Fig. 6b, curve *2*; Table 3) and the two other peaks occur at temperatures 40–70°C lower.

The iron-containing systems are similar in reduction behavior to the manganese-containing systems. The TPR reduction spectrum of $Ce_{0.20}Zr_{0.64}Fe$ shows three peaks at 205, 450, and 730°C (Fig. 6a, curve *3*). The reduction of iron oxide is a two-step process: $Fe_2O_3 \longrightarrow Fe_3O_4 \longrightarrow$ α-Fe [19]. The first-step reduction temperature ranges between 300 and 400°C, depending on the nature of the support; the second-step reduction temperature varies between 400 and 600°C. Therefore, iron in the systems examined is in a state other than oxide. The $Ce_{0.33}Zr_{0.51}Fe$ sample is reduced at higher temperatures of 500, 780, and 840°C (Fig. 6b, curve *3*; Table 3).

The introduction of cobalt gives rise to a low-temperature peak at 140°C (Figs. 6a, 6b, curves *4*), irrespective of the cerium content of the sample, and shifts the second peak to lower temperatures by 170–190°C relative to the same peak for the unpromoted sample. The third-peak temperature changes only slightly (Table 3). Therefore, cobalt reduction also proceeds in two steps. This assumption is supported by the report that cobalt-containing perovskite is reduced in two steps taking place at 387 and 527°C [20]:

$$Co^{3+} \longrightarrow Co^{2+}, \quad \text{(I)}$$

$$Co^{2+} \longrightarrow Co^0. \quad \text{(II)}$$

The reduction behavior of the systems depends on the conditions under which they were synthesized. In particular, the manganese-containing sample precipitated at 70°C and calcined at 600°C is reduced in three steps. However, all three reduction peaks occur at lower temperatures than the peaks for a sample of similar composition precipitated at ~23°C (Table 3). A different dependence is observed for iron-containing samples of similar compositions. An analysis of their TPR profiles (Fig. 7) shows that the iron-containing sample precipitated at ~23°C is reduced at temperatures approximately 100°C lower (605 and 650°C) than the sample prepared at 70°C (710°C).

Furthermore, the reduction behavior of the systems depends strongly on the calcination temperature. For the $Ce_{0.30}Zr_{0.55}Mn$ sample, raising the calcination temperature from 600 to 1150°C causes the disappearance of the low temperature peak at 180°C and shifts the two other peaks to higher temperatures, one from 505 to 765°C and the other from 760 to 840°C (Table 3). This increase in the reduction temperatures is possibly due to the fact that the specific surface area decreases greatly at 1150°C, implying that reduction will primarily involve bulk phases, whose reduction temperatures are higher.

Thus, the above data suggest that the most effective reducibility-enhancing component is cobalt. Furthermore, a transition metal introduced into the cerium–zirconium oxide system facilitates the reduction of surface Ce^{4+} ions and does not affect the reduction of Ce^{4+} in the bulk.

According to the equation $2CeO_2 + H_2 \longrightarrow Ce_2O_3 + H_2O$, the reduction of 1 g of CeO_2 requires 2.92 mmol of H_2. Based on this value, we calculated the amount of hydrogen necessary to reduce the CeO_2 present in the catalysts (Table 3). In similar ways, we calculated the amounts of hydrogen necessary for the reduction of the manganese, iron, and cobalt oxides in the catalysts, assuming that the manganese cation is reduced to Mn^{2+} and the iron and cobalt cations are reduced to metals. Table 3 lists the observed and calculated amounts of hydrogen consumed in the reduction of the samples. Clearly, hydrogen consumption is raised by introducing a transition metal into the cerium–zirconium oxide system. Furthermore, it increases with increasing cerium content and decreases with increasing precipitation and calcination temperatures. The extent of reduction (α) of the samples calcined at 600°C decreases in the order CeZr $\longrightarrow$ CeZrMn $\longrightarrow$ CeZrFe $\longrightarrow$ CeZrCo, irrespective of the component ratios. Note that $\alpha > 1$ for some samples calcined at 600°C. It is likely that this effect arises from the fact that the fluorite-type solid solution formed at this temperature consists of very small particles ($D \approx 40$–50 Å) and has a larger unit cell parameter than is observed for the sample calcined at 1150°C (Table 2). Accordingly, the above differences in α are due to the contribution from the surface into the reduction of these samples.

Since the overall hydrogen consumption characterizes the relative amount of oxygen thermodynamically available at a given temperature [21], its increase suggests that the catalysts based on the cerium–zirconium oxide system promoted with a transition metal will be more efficient.

Catalytic Properties

The catalytic properties of the samples calcined at 600°C were studied in the oxidation of hydrocarbons (HC) and CO and in the reduction of NO at various values of the redox potential *R*. Figure 8 plots the HC, CO,

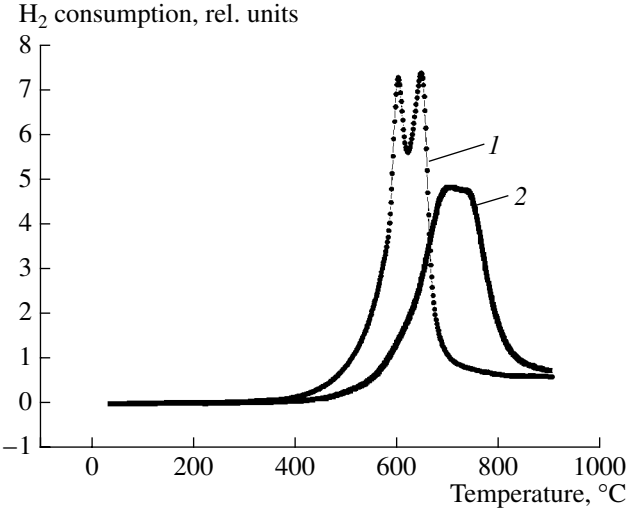

Fig. 7. TPR profiles for iron-containing samples precipitated at (*1*) 23 and (*2*) 70°C and calcined at 1150°C.

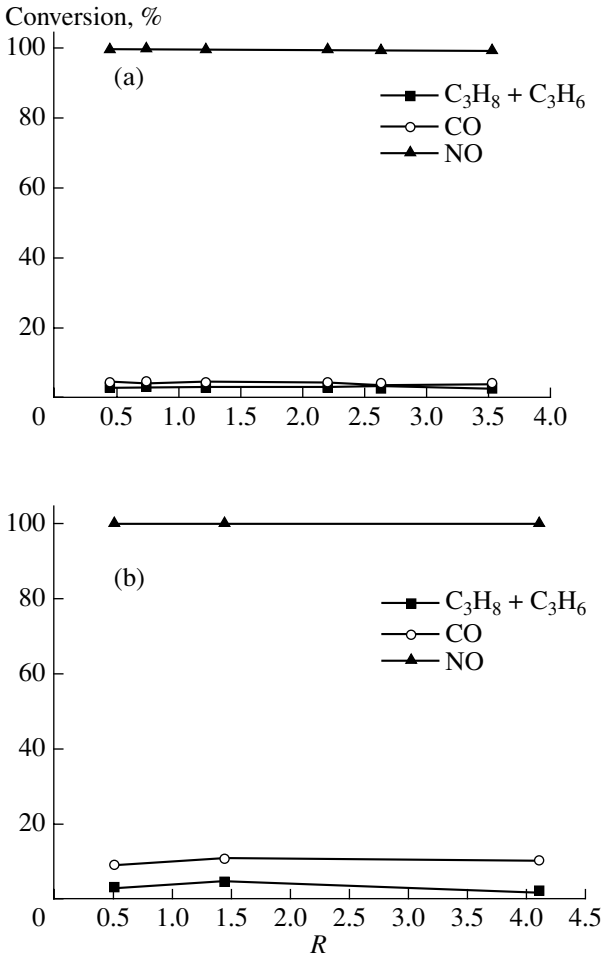

Fig. 8. HC, CO, and NO conversions on (a) $Ce_{0.18}Zr_{0.69}$ and (b) $Ce_{0.22}Zr_{0.61}Co$ calcined at 600°C versus the redox potential of the reaction system.

Table 4. Catalytic properties of cerium–zirconium systems promoted with transition metals*

Sample	T_{react}, °C	R	Conversion, %		
			C_3H_8	CO	NO
$Ce_{0.18}Zr_{0.69}$	400	3.53	3.1	4.1	100
		2.62	3.4	3.9	100
		2.19	3.2	4.0	100
		1.21	2.9	4.5	100
		0.73	3.2	4.2	100
		0.44	3.0	4.4	100
$Ce_{0.21}Zr_{0.64}$**Mn**	400	3.93	2.9	3.6	100
		1.23	2.9	3.2	100
		0.42	2.7	3.5	100
	450	0.42	2.8	3.4	100
$Ce_{0.20}Zr_{0.64}$**Fe**	400	3.46	0	6.3	100
		1.14	0	5.4	100
		0.39	0	6.0	100
	450	0.43	0	13.1	100
$Ce_{0.22}Zr_{0.61}$**Co**	400	4.09	1.6	10.1	100
		1.43	2.5	10.6	100
		0.50	2.9	9.2	100
	450	0.49	4.3	19.2	100
$Ce_{0.29}Zr_{0.64}$	400	3.64	0.0	0.2	100
		1.34	0.7	0.4	100
		0.49	0.0	1.2	100
	450	0.48	0.1	0.0	100
$Ce_{0.30}Zr_{0.55}$**Mn**	400	4.03	1.2	11.2	100
		2.52	2.3	12.4	100
		1.41	2.7	15.1	100
		0.51	2.3	15.0	100
	450	0.51	0.0	17.0	100
$Ce_{0.30}Zr_{0.57}$**Co**	400	4.38	0.9	13.5	100
		3.37	0.3	15.2	100
		1.58	0.5	15.7	99.9
		0.59	0.7	15.9	99.9
	450	0.57	1.7	28.3	99.9

* The samples were calcined at 600°C.

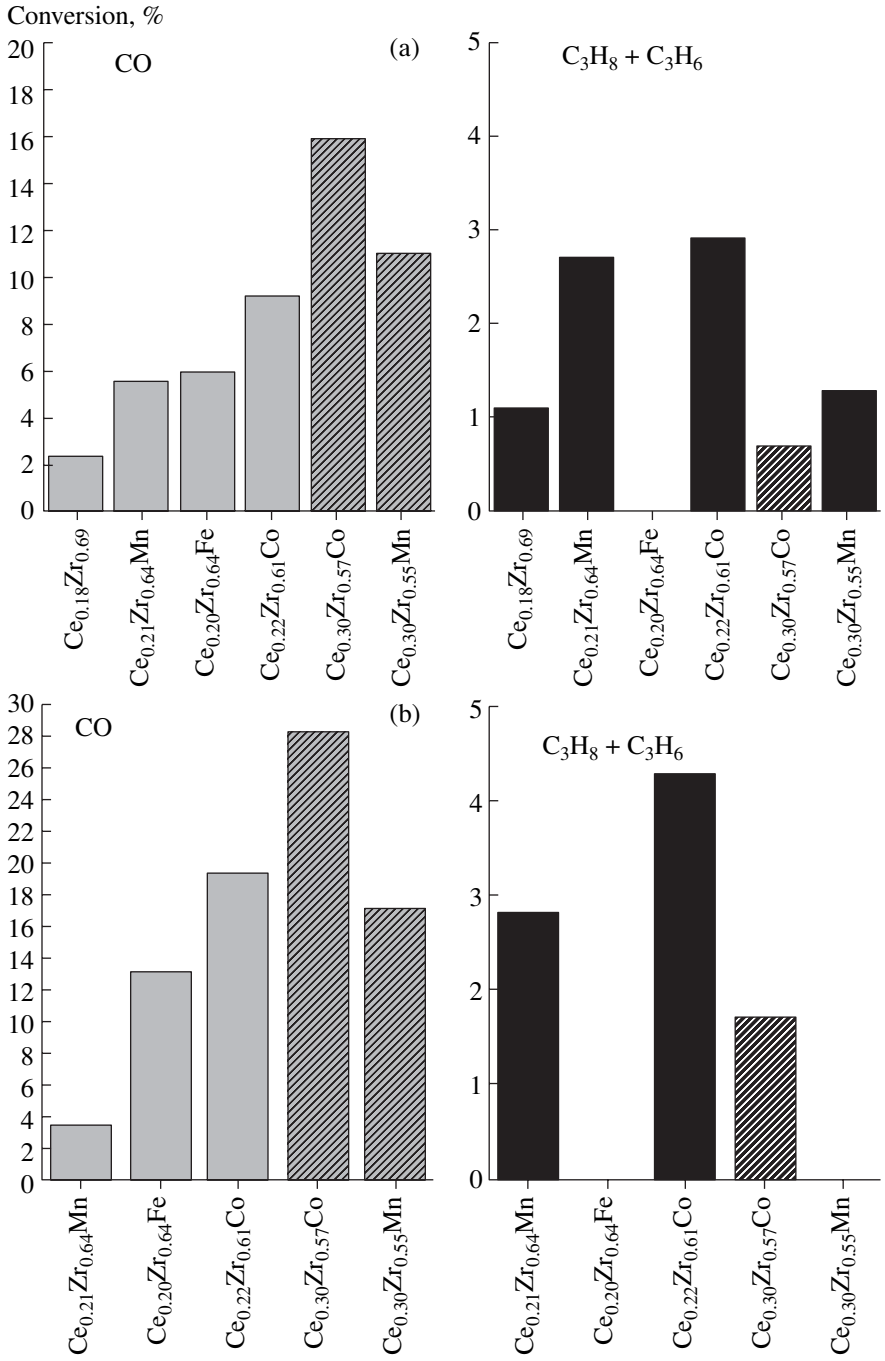

Fig. 9. Dependence of the activity of fluorite-type catalysts on the nature of the transition metal at $R = 0.5$ and $T =$ (a) 400 and (b) 450°C.

and NO conversions versus R for catalysts differing in component ratios and transition metal. The corresponding numerical data are presented in Table 4. The data listed in Table 4 suggest that the catalysts with a fluorite structure that contain no noble metal show low activity in HC and CO oxidation and are active in NO reduction. Irrespective of the catalyst, the NO conversion at 400 and 450°C is ~100%. The HC and CO conversions are governed by the catalyst composition.

For the unpromoted catalyst $Ce_{0.18}Zr_{0.69}$, the HC and CO conversions at 400°C are 3.2 and 4.2%, respectively, and are independent of R (Table 4). The $Ce_{0.29}Zr_{0.64}$ sample, which is richer in cerium, is almost inactive in HC and CO oxidation at both 400 and 450°C.

Introducing a transition metal into the cerium–zirconium oxide systems changes their activity in HC and CO oxidation, which, however, remains independent

of R. For catalysts with similar Ce/Zr ratios, the HC and CO conversions at 400°C changes in the following order (Table 4):

HC: $Ce_{0.21}Zr_{0.64}\mathbf{Mn} \approx Ce_{0.22}Zr_{0.61}\mathbf{Co} > Ce_{0.20}Zr_{0.64}\mathbf{Fe}$;

CO: $Ce_{0.22}Zr_{0.61}\mathbf{Co} > Ce_{0.20}Zr_{0.64}\mathbf{Fe} > Ce_{0.21}Zr_{0.64}\mathbf{Mn}$.

Raising the reaction temperature to 450°C increases the CO conversion only on the Co- and Fe-containing catalysts (Table 4) and exerts no effect on the CO conversion on the Mn-containing catalyst. These activity trends are also observed for samples with a higher cerium content ($Ce_{0.30}Zr_{0.55}$Mn and $Ce_{0.30}Zr_{0.57}$Co): the HC conversion on these catalysts is nearly the same as the HC conversion on the catalysts with a lower cerium content ($Ce_{0.21}Zr_{0.64}$Mn and $Ce_{0.22}Zr_{0.61}$Co), while the CO conversion is as high as 15%. Figure 9 compares HC and CO conversions at $R = 0.5$ and $T = 400$ and 450°C. The cobalt-containing catalysts are the most active: $Ce_{0.22}Zr_{0.61}$Co is the most active in HC oxidation; $Ce_{0.30}Zr_{0.57}$Co, in CO oxidation. These data are in agreement with our TPR data, which indicate that other conditions being equal, the first-peak temperature decreases in the order

	$Ce_{0.21}Zr_{0.64}\mathbf{Mn}$	>	$Ce_{0.20}Zr_{0.64}\mathbf{Fe}$	>	$Ce_{0.22}Zr_{0.61}\mathbf{Co}$
T, °C	270	>	205	>	140;

that is, the higher the reducibility of the catalyst, the higher the probability of weakly bound oxygen present on the catalyst surface and, accordingly, the higher the extent of total HC and CO oxidation.

Thus, our study has demonstrated that the cerium–zirconium systems promoted not only with a rare-earth metal (Y or La) but also with a transition metal (Mn, Fe, or Co) are more active in hydrocarbon and carbon monoxide oxidation than the systems containing no transition metal. Therefore, in the synthesis of Pt(Pd)/$Ce_{1-x}Zr_xO_2$/support three-way catalysts, it is pertinent to use transition metal–containing systems of composition Pt(Pd)/$Ce_{1-x-y-z}Zr_x(Y,La)_y M_zO_{2-\delta}$/support (M = Mn, Fe, Co). As is noted above, three-way catalysts are most active at a stoichiometric fuel/air ratio. Changing the reducer-to-oxidizer ratio (R) in the reaction mixture from 3.5–4.0 to 0.39–0.50 does not cause any appreciable changes in the activity of the $Ce_{1-x-y-z}Zr_x(Y,La)_yM_zO_{2-\delta}$ systems. Two plausible explanations are suggested for this fact. Firstly, the systems are less readily reduced with the reaction mixture than with H_2 and, as a consequence, are insensitive to the R value. Secondly, the absence of a noble metal, which would enhance the reducibility of both M^{3+} and Ce^{4+} [22–24], also diminishes the efficiency of the catalysts.

REFERENCES

1. Kaspar, J., Fornasiero, P., and Graziani, M., *Catal. Today*, 1999, vol. 50, p. 285.
2. Kirchner, T. and Eigenberger, G., *Catal. Today*, 1997, vol. 38, p. 3.
3. Tagliaferri, S., Koppel, R.A., and Baiker, A., *Appl. Catal., B,* 1998, vol. 15, p. 159.
4. Ikryannikova, L.M., Aksenov, A.A., Markaryan, G.L., Murav'eva, G.P., Kostyuk, B.G., Kharlanov, A.N., and Lunina, E.V., *Appl. Catal., A*, 2001, vol. 210, p. 225.
5. Kulyova, S.P., Lunina, E.V., Lunin, V.V., Kostyuk, B.G., Muravyova, G.P., and Kharlanov, A.N., *Chem. Mater.*, 2001, vol. 13, p. 91.
6. Lunina, E.V., Lunin, V.V., Zhilinskaya, E.A., and Aboukais, A., *Colloids Surf., A*, 1999, vol. 151, p. 5.
7. Jen, H.-W., Graham, G.W., Chun, W., McCabe, R.W., Cuif, J.-P., Deutsch, S.E., and Touret, O., *Catal. Today*, 1999, vol. 50, p. 309.
8. Lamonier, C., Ponchel, A., D'Huysser, A., and Jalowiecki-Duhamel, L., *Catal. Today*, 1999, vol. 50, p. 247.
9. Takeguchi, T., Furukama, S., and Inoue, M., *J. Catal.*, 2001, vol. 202, p. 14.
10. Price, W.J., *Analytical Atomic Absorption Spectroscopy*, London: Heyden, 1972.
11. Kraus, W. and Nolze, G., *CPD Newsletter*, 1998, vol. 20, p. 27.
12. Solov'eva, L.P., Tsybulya, S.V., and Zabolotnyi, V.A., *Polikristall—sistema programm dlya strukturnykh raschetov* (Polikristall: Program Package for Structure Calculations), Novosibirsk: Inst. Kataliza, 1988.
13. Buyanova, N.E., Karnaukhov, A.P., and Alabuzhev, Yu.A., *Opredelenie udel'noi poverkhnosti dispersnykh i poristykh materialov* (Determination of the Surface Area of Disperse Porous Materials), Novosibirsk: Inst. Kataliza, 1978.
14. Yao, H.C. and Yu, YaoY.F., *J. Catal.*, 1984, vol. 86, p. 254.
15. Trovarelli, A., *Catal. Rev. Sci. Eng.*, 1996, vol. 38, p. 439.
16. Zviadadze, G.N., Koryazina, I.N., Mel'nik, Yu.I., Nevzorova, O.V., and Makarov, Yu.B., in *Diffuziya, sorbtsiya i fazovye prevrashcheniya v protsessakh vosstanovleniya metallov* (Diffusion, Sorption, and Phase Transitions in Metal Reduction), Tsvetkov, Yu.V., Ed., Moscow: Nauka, 1981.
17. Kapteijn, F., Singoredjo, L., Andreini, A., and Moulijn, J.A., *Appl. Catal., B*, 1994, vol. 3, nos. 2–3, p. 173.
18. Van de Kleut, D., *Ph.D. Thesis*, Utrecht, the Netherlands: University of Utrecht, 1994.
19. Chernavskii, P.A., Pankina, G.V., Zavalishin, I.N., and Lunin, V.V., *Kinet. Katal.*, 1994, vol. 35, no. 1, p. 126.
20. Fierro, J.L.G., Pena, M.A., and Tejuca, L.G., *J. Mater. Sci.*, 1988, vol. 23, p. 1018.
21. Fornasiero, P., Di Monte, R., Rao, G.R., Kaspar, J., Meriani, S., Trovarelli, A., and Graziani, M., *J. Catal.*, 1995, vol. 151, p. 168.
22. Sermon, P.Q. and Bond, G.C., *Catal. Rev.*, 1973, vol. 8, p. 211.
23. Bianchi, D., Gardes, G.E., Pajonk, G.M., and Teichner, S.J., *J. Catal.*, 1975, vol. 38, p. 135.
24. Imamura, S., Higashihara, T., Saito, Y., Aritani, H., Kanai, H., Matsumura, Y., and Tsuda, N., *Catal. Today*, 1999, vol. 50, p. 369.